ADVANCED MATERIALS

Supporting Information

for *Adv. Mater.*, DOI 10.1002/adma.202302765

Liquid Crystal Elastomer–Liquid Metal Composite: Ultrafast, Untethered, and Programmable Actuation by Induction Heating

*Victor Maurin, Yilong Chang, Qiji Ze, Sophie Leanza, Jing Wang and Ruike Renee Zhao**

Supporting Information

Liquid Crystal Elastomer - Liquid Metal Composite: Ultrafast, Untethered, and Programmable Actuation by Induction Heating

*Victor Maurin, Yilong Chang, Qiji Ze, Sophie Leanza, Jing Wang, Ruike Renee Zhao**

Table of content

Supplementary methods

Material characterizations

Material characterizations are performed to determine the properties of the liquid crystal elastomer (LCE) and of the thermally inactive material (Elastic 50A Resin, Formlabs Inc., USA) used for the demonstrations in this paper. To determine the temperature vs. strain relationship of the LCE, a dynamic mechanical analyzer (DMA 850, TA instruments, USA) is used to measure the contraction strain in the alignment direction of a 3D-printed single-layer LCE sample with dimensions of 30 mm × 5 mm × 0.2 mm with longitudinally aligned mesogens. The sample is first preloaded with a 0.01 N force along its longitudinal direction, and then heated to 160°C. After that, the sample is gradually cooled to 30°C at a rate of 3°C min^{-1} while keeping the force constant. During the cooling process, the temperature vs. strain relationship of the LCE sample is recorded, as shown in **Figure S1A**. A dynamic mechanical analysis (DMA) is also performed on the LCE. A 3D-printed sample of size 25 mm × 5 mm × 0.7 mm with longitudinally aligned mesogens is first cooled to -50°C and stabilized for 3 min to reach thermal equilibrium. A preload of 5 mN is applied, and the strain is oscillated at a frequency of 1 Hz with a peak-to-peak amplitude of 0.1% along the LCE alignment direction. The temperature increases from -50°C to 135°C at a rate of 3°C min^{-1}. The results of the DMA test are shown in **Figure S1B**. To obtain the Young's modulus of the LCE at 120°C, a uniaxial tensile test is conducted using a dynamic mechanical analyzer. A 3D-printed LCE sample with dimensions of 25 mm × 5 mm × 0.7 mm and longitudinal mesogen alignment is stretched to 25% strain at a strain rate of 0.01 s^{-1} along the alignment direction, at a temperature of 120°C. The temperature is first raised to 120°C and stabilized for 5 min. The test is then performed. A shear modulus of 507 kPa is estimated based on a neo-Hookean fit of the data, as shown in **Figure S1C.** The LCE Young's modulus is calculated to be ~1.5 MPa at 120°C due to the

assumption of material incompressibility (Poisson's ratio of 0.5). To determine the Young's modulus of the thermally inactive material at room temperature, a uniaxial tensile test is conducted using a universal testing machine (3344, Instron Corp., USA). A rectangular sample with dimensions of 30 mm × 10 mm × 2 mm is loaded along its longitudinal direction and stretched to 25% strain at a strain rate of 0.01 s^{-1}. A shear modulus of 890 kPa is estimated based on a neo-Hookean fit of the data, as shown in **Figure S1D**. Assuming that the material is also incompressible (Poisson's ratio of 0.5), a Young's modulus of ~2.7 MPa is calculated. To characterize the thermal stability of the LCE at different temperatures, a thermogravimetric analysis (TGA) (TGA5500, TA instruments, USA) is performed on a 3 mm × 3 mm × 0.15 mm 3D-printed LCE sample, with an initial weight of 11.5 mg. The sample is tested at temperatures ranging from 25°C to 600°C, with a temperature increase rate of 10°C min^{-1}. The results are shown in **Figure S1E**.

LCE-LM composite interfacial adhesion characterization

A 90° peel test is performed to characterize the bonding and adhesion of the LCE-LM composite manufactured as shown in **Figure S2**. The composite tested is made of two LCE layers with 30 mm × 12 mm × 0.15 mm size, and a rectangular LM pattern with 6 LM layers and 25 mm × 9 mm size. The test is realized with a tensile test machine (3344, Instron Corp. USA), at a rate of 2.5 mm/min. The test schematic is provided in **Figure S3A**. During the test, the bottom LCE layer is fixed, and the top LCE layer is attached to the machine's grips. Three snapshots taken during the test are shown in **Figure S3B**, where we can see the top layer of the composite being stretched by the tensile test machine. The obtained results of the test are shown in **Figure S3C**. As illustrated in **Figure S3D**, two pictures of the sample tested have been taken before the test (left picture), and after the test (right picture).

Temperature distribution measurement

All the temperature distributions from experiments are recorded using an IR thermal camera (Fotric 348A, Fotric Inc., USA). For the measurements in Figure 2, certain thicknesses of LM are coated on a 0.2 mm thick glass slide by spraying specific numbers of LM layers through a paper mask with a 15 mm × 15 mm square cut. After the mask is removed, a 0.2 mm thick glass slide is placed on top of the LM sprayed to reduce its reflection for better temperature distribution visualization with the thermal camera. The camera emissivity is calibrated as 0.93 after comparing the temperature measured with the thermal camera and a thermocouple placed on the top of the glass slide. For Figure 3 and Figure 4, the temperature is recorded directly from the LCE samples without adding the top glass slide, since the LM is covered by the LCE layer. The camera emissivity is set to 0.98 after calibration using the same method, with the thermocouple placed on the top LCE layer.

Selection of coils for different demonstrations

In this paper, two different helical coils and three different spiral coils are used for the demonstrations. Compared to spiral coils, helical coils can generate a relatively uniform magnetic field at their center, which can be verified by the simulation results shown in **Figures S4 - S8**. A uniform magnetic field is preferred for the characterizations of LM induction heating. To make sure that the different regions of the single LM square in Figure 2A - 2C and the different LM squares in Figure 2E can be inductively heated under similar conditions, two helical coils with variable inner diameters are selected based on the sample dimensions. For all other demonstrations that do not involve heating characterizations, having a uniform magnetic field is less important. Spiral coils are thus selected for their merits concerning 1) selective heating of a targeted sample region, 2) heating of samples that are larger than the coil dimensions, 3) heating of samples that may deform or move out of the coil region. For the

demonstrations shown in Figure 3, 4 and 5, three different spiral coils with varying dimensions are therefore selected depending on the specific LM region that needs to be heated. When the shape and dimension of the coil is chosen, the coil is then connected to the induction heater to generate the desired alternating magnetic field. The frequency of the alternating magnetic field is determined by the LC resonant circuit inside the induction heater. As the design of the coil is determined, the values of the capacitor (C) and inductance (L) are fixed, which means that the frequency of the coil is set. The operating frequencies of the five coils used in this paper are highlighted in **Table S1**. The strength of the magnetic field can be adjusted by tuning the current flowing through the coil.

Electromagnetic finite element analysis

The commercial software Ansys Maxwell (Ansys Inc., USA) is utilized for the induction heating finite element analysis (FEA) to predict the induced ohmic losses and to guide the LCE-LM composite design. In the software, the eddy current is calculated by applying the measured alternating magnetic field frequency as shown in **Table S1**. Note that the frequency is recorded directly from the coil using an AC probe (i1000s, Fluke Corp., USA) connected to an oscilloscope (EDUX1002A, Keysight Technologies Inc., USA). Both coils and LM layers with their specific thicknesses are included in the FEA models to simulate the real experimental conditions of the demonstrations in Figure 2 - Figure 4. The relative permeability and conductivity of the materials used for simulations are listed in **Table S2**. For all demonstrations using helical coils, the LM samples are placed at the center of the coils. For other demonstrations using spiral coils, the LM samples are placed on a plane 2 to 3 mm above the corresponding coils. The magnetic field distributions on the planes of the LM samples are simulated and shown in **Figures S4 - S8**. In the main text, the given magnetic field values are the magnetic field values at the sample position (highlighted in red in **Figures S4 - S8**). The ohmic loss distributions of the samples are exported and shown in the figures of the main text.

The total ohmic loss is calculated by integrating the ohmic loss distribution over the volume of the LM.

Liquid metal layer thickness characterization

The thickness of the liquid metal (LM) pattern is controlled by the number of LM layers sprayed. For each LM layer, the LM is sprayed on the substrate by pressing the airbrush with an approximate 5 cm distance from the substrate and at a pressure of 1.5 bar for 1 s. To determine the relationship between the LM thickness and the number of LM layers, we prepare samples with 2, 4, 6, 8, 10, 20, and 30 LM layers. For samples with 2, 4, 6, and 8 layers, we spray the desired amount of LM onto a 0.2 mm thick glass slide. A microscope (AM Scope Inc., USA) is then used to determine the thickness of those samples. For samples with 10, 20 and 30 LM layers, we sandwich the LM between two 0.2 mm glass slides to obtain a uniform thickness. The thickness of those samples is then directly measured. The results of the thickness in terms of the number of LM layers applied are summarized in **Figure S9A**. Pictures of the 10, 20 and 30 LM layers samples are shown in **Figure S9B**, **Figure S9C**, and **Figure S9D**, as well as their measured thicknesses, equal to 115 μm, 195 μm and 320 μm, respectively.

Specific heat calculations

To guide the design of the LM pattern thickness to enable sequential heating under an increasing magnetic field amplitude, the critical ohmic loss for a specific LM pattern is calculated based on the specific heat equation. Above the critical ohmic loss, the total ohmic loss generated by induction heating is able to heat the LCE layers of the LCE-LM composite above the temperature corresponding to a desired actuation. The critical ohmic loss formula is as follows:

$$P = \frac{Q}{\Delta t} = \frac{\rho V c \Delta T}{\Delta t} \tag{1}$$

where P is the critical ohmic loss, Q is the energy absorbed by the LCE, Δt is the duration of heating, ρ is the density of the LCE, V is the volume of the LCE heated, c is the specific heat capacity of the LCE, and ΔT is the temperature difference of the LCE before and after heating. Note that P represents the power required for heating a given volume of LCE by a temperature ΔT in a time Δt.

For all the calculations, the following parameter values are used: ρ is calculated as 1.1 g cm^{-3} after measuring the weight and the volume of an LCE sample. c is set as 1 J K^{-1} g^{-1} based on the literature.[1] Δt is set to 2 s for fast heating. Finally, ΔT and V are chosen depending on the temperature we want to achieve and the dimensions of the LCE-LM composite heated, respectively.

For the demonstration in Figure 2E, the critical ohmic loss is calculated as the required total ohmic loss from a single LM square to heat an LCE-LM composite above 120°C for full actuation (40% strain, see **Figure S1A** for the temperature vs. strain curve of the LCE). Two LCE layers in the LCE-LM composite, each with a dimension of 15 mm × 15 mm × 0.15 mm, are considered for calculations. Note that the thickness of 0.15 mm is chosen based on measurements of LCE layers after direct ink writing, and the size of 15 mm × 15 mm is equal to the size of each LM square. Considering the initial temperature of the LCE to be 20°C (room temperature), ΔT should be at least 100°C for the LM square to achieve a temperature above 120°C for actuating the LCE-LM composite. With these values, the critical ohmic loss is computed as 3.7 W. Figure 2E demonstrates the ohmic loss of the LM squares under an increasing magnetic field. Similar calculations are performed for the pop-up structure sequential heating demonstrated in Figure 4.

Thermo-structural finite element analysis

FEA simulations are performed to guide the structural design of the LCE-LM composite using the commercial software ABAQUS 2021 (Dassault Systèmes, France). Model dimensions, modulus, density, thermal conductivity, specific heat capacity, orthotropic thermal expansion coefficients of the LCE, as well as applied temperature are the inputs to predict the thermal actuation of each LCE-LM design. For the LCE, an isotropic linear elastic model is used with Young's modulus of 1.5 MPa (value recorded at 120°C, as shown in **Figure S1C**), Poisson's ratio of 0.49, a density of 1.1 g cm^{-3}, a conductivity of 0.3 W K^{-1} m^{-1},[2] and a specific heat of 1 J K^{-1} g^{-1}.[1] the LCE shows approximately -6%, -32%, and -41% strain along the alignment direction at temperatures of 60, 100, and 140°C, respectively (**Figure S1A**, the reference temperature is 20°C in the simulations). The temperature vs. strain relationship is modeled with orthotropic thermal expansion coefficients (**Table S3**, note that Alpha 11 is the thermal expansion coefficient along the fiber direction. Alpha 22 and Alpha 33 are thermal expansion coefficients in directions orthogonal to the alignment direction). A small damping factor (10^{-6} to 10^{-4}) is adopted in the simulation to help with the convergence. The LM region is not considered in the simulation as it does not impose constraints on the LCE deformation. The heating is directly imposed at the LCE-LM interfaces in the different composites of this paper.

For the LCE-LM bilayer structure simulation demonstrated in Figure 3, the element C3D8HT is applied including gravity and frictionless contact with a substrate. The thermally inactive material is modeled to have Young's modulus of 2.7 MPa (as shown in **Figure S1D**) with a 0.49 Poisson's ratio. Heating is directly applied to the surface on which the LCE and LM interface. The bilayer structure is discretized into a 3 × 14 grid (**Figure S10**). In total, eleven coupled temperature-displacement steps are created. A non-uniform heating pattern is adopted at each step to mimic the heat distribution observed in Figure 3B. In the first step, the first 5 blocks on the first and third rows are heated from 20°C to a temperature of 80, 140, 140, 140,

and 80°C, respectively, whereas the rest of the blocks in these two rows remain at 20°C. For the middle row, the first 5 blocks are heated from 20°C to 40, 100, 100, 100, and 40°C respectively whereas the rest of the blocks in this row remain at 20°C. For the following steps, the heating pattern on each row moves one block to the right along the longitudinal direction of the structure. The blocks that are outside of the heated region are cooled down to 20°C.

For the simulation of the pop-up structure demonstrated in Figure 4, the element C3D8HT is used. Two coupled temperature-displacement steps are created, which include gravity and frictionless contact with a substrate. The LCE surface in contact with 20 layers of LM (inner LM circle) is heated from 20°C to 140°C at the first heating step. In the second step, the LCE surfaces that interact with the 6-layer LM region (outer LM ring segments) are heated from 20°C to 140°C while the heated region in the first step remains at 140°C.

For the actuation of the fin demonstrated in Figure 5, element C3D8HT is used. Two coupled temperature-displacement steps are created including gravity and frictionless contact with the substrate. The interface of LM and LCE is heated to 140°C and cooled down to 20°C. For the turtle motion simulations demonstrated in Figure 5, element C3D8HT is used. The turtle body is modeled to have Young's modulus of 1 GPa, Poisson's ratio of 0.3, and a density of 1 g cm^{-3}. The fin is tied to the turtle's body on two sides by tie constraints. Frictionless contact is applied between the turtle body, fins, as well as the substrate they are placed on. The heat is applied to the LM and LCE interfaces. For the walking motion, three coupled temperature-displacement steps are created. The LM and LCE interfaces of the two fins are heated to 140°C instantaneously from 20°C, then a region of the front of each fin is fixed to mimic friction contact with the substrate, and finally, the LM surface is cooled from 140°C to 20°C while the fix constraint on the fin is removed. For the turtle turning motion, similarly, three coupled temperature-displacement steps are created. For turning right, only the LM and LCE interface

of the left fin is heated and cooled, and only a region on the left fin front is fixed and unfixed respectively. A similar process is realized for the turning left motion on the right fin.

Supplementary Figures S1-S10

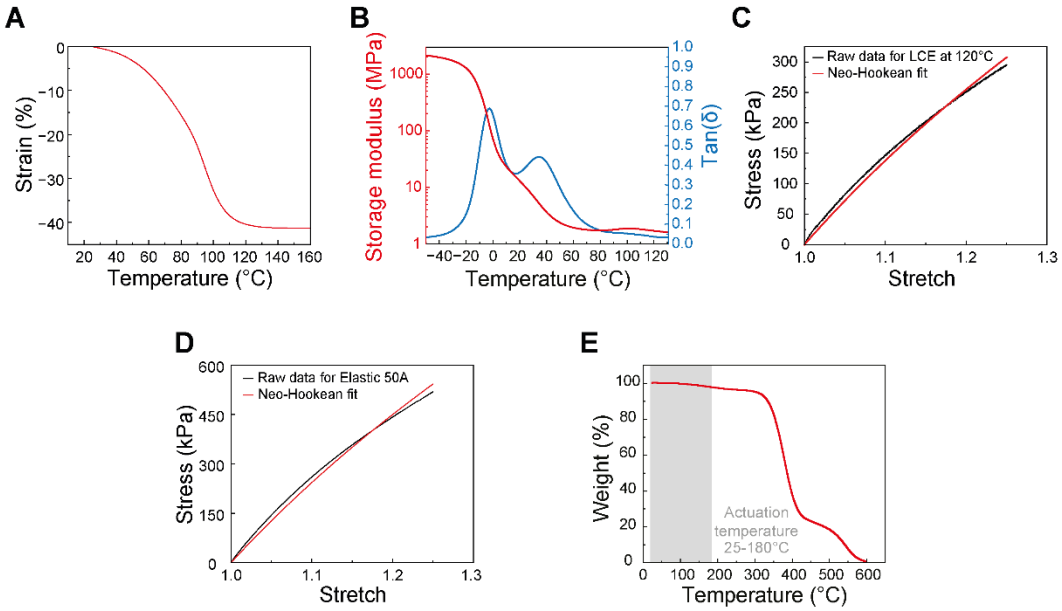

Figure S1. Material characterizations of the LCE and thermally inactive material. (A) temperature vs. strain curve of the LCE. (B) DMA characterizations of the LCE. Tensile test curves of (C) the LCE at 120°C and (D) the thermally inactive material (Elastic 50A) at room temperature. The raw data are fitted with the neo-Hookean model. The shear moduli of the LCE at 120°C and of the thermally inactive material at room temperature are estimated as 507 kPa and 890 kPa, respectively. (E) TGA characterizations of the LCE. The actuation temperature range of the composite is highlighted in grey.

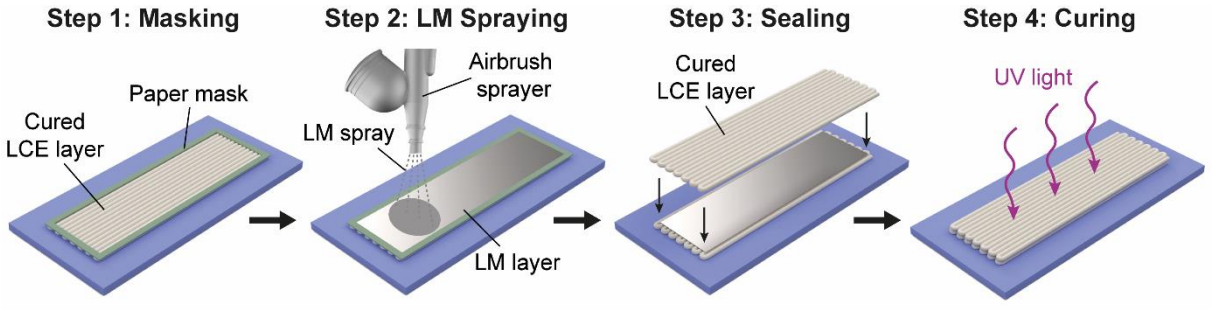

Figure S2. Fabrication steps of the LCE-LM composite.

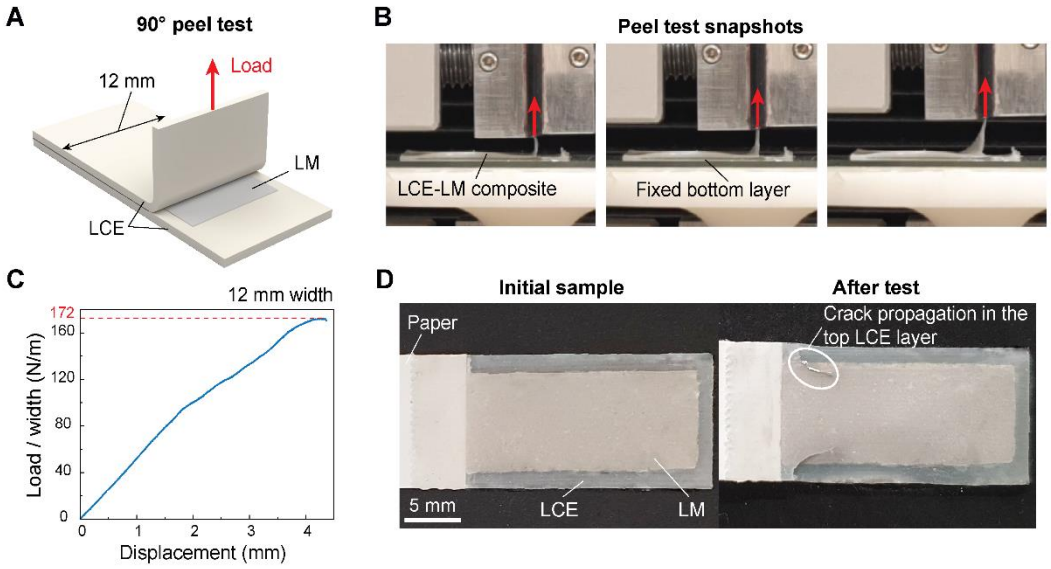

Figure S3. 90° peel test of the LCE-LM composite. (A) 90° peel test schematic. The load direction is indicated by the red arrow. (B) Three snapshots taken during the peel test. (C) Plot of the applied tensile load divided by the width of the sample versus the displacement of the moving grips. The original sample width is 12 mm. A maximum load of 172 N/m is recorded. (D) Sample before the test (left picture) and after the test (right picture). A paper is inserted between the LCE layers to prevent their bonding during manufacturing. At the end of the test, a crack has propagated inside the top LCE layer. No obvious debonding is observed. Scale bar: 5 mm.

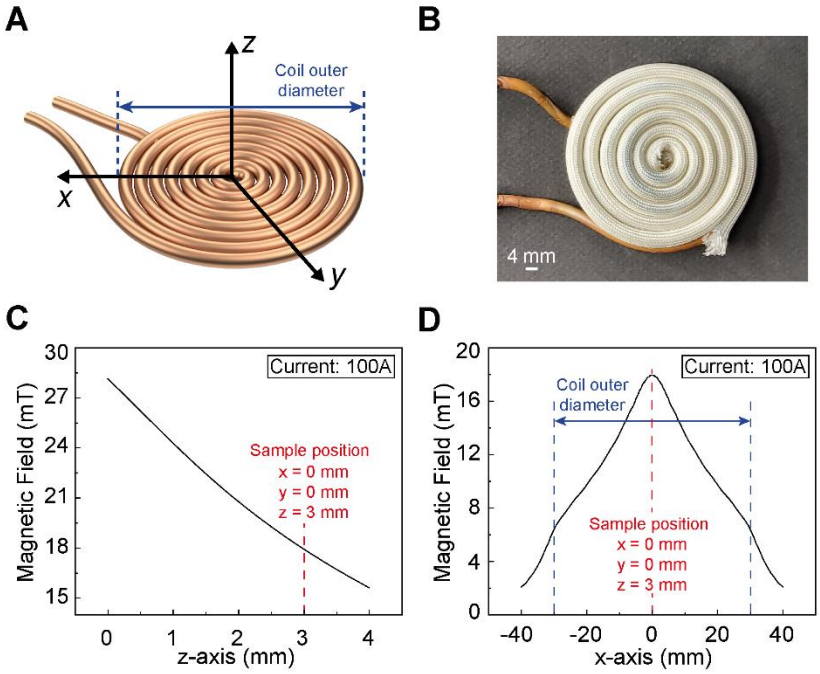

Figure S4. Magnetic field distribution of the spiral coil used in Figure 1 & Figure 5. (A) Schematic of the coil. The outer diameter of the coil is highlighted in dark blue. (B) Picture of the coil. Magnetic field distribution at a current of 100 A along (C) the z-axis, which is measured from the top surface of the coil, and (D) the x-axis, which is measured along the coil outer diameter. The sample position is highlighted in red on both curves.

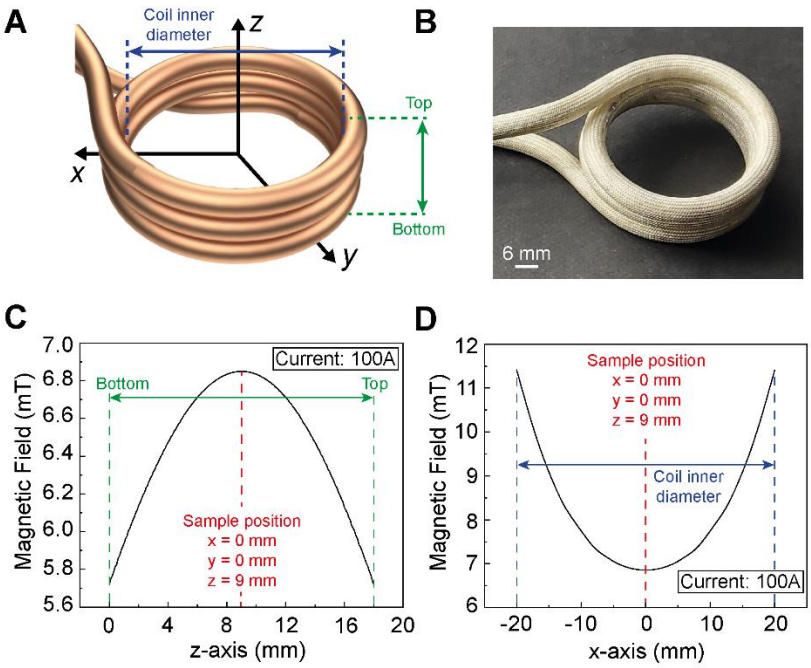

Figure S5. Magnetic field distribution of the helical coil used in Figure 2A - 2C. (A) Schematic of the coil. The inner diameter of the coil is highlighted in dark blue. The top and bottom of the coil are highlighted in green. (B) Picture of the coil. Magnetic field distribution at a current of 100 A along (C) the z-axis, which is measured from the bottom to the top of the coil, and (D) the x-axis, which is measured along the coil inner diameter. The sample position is highlighted in red on both curves.

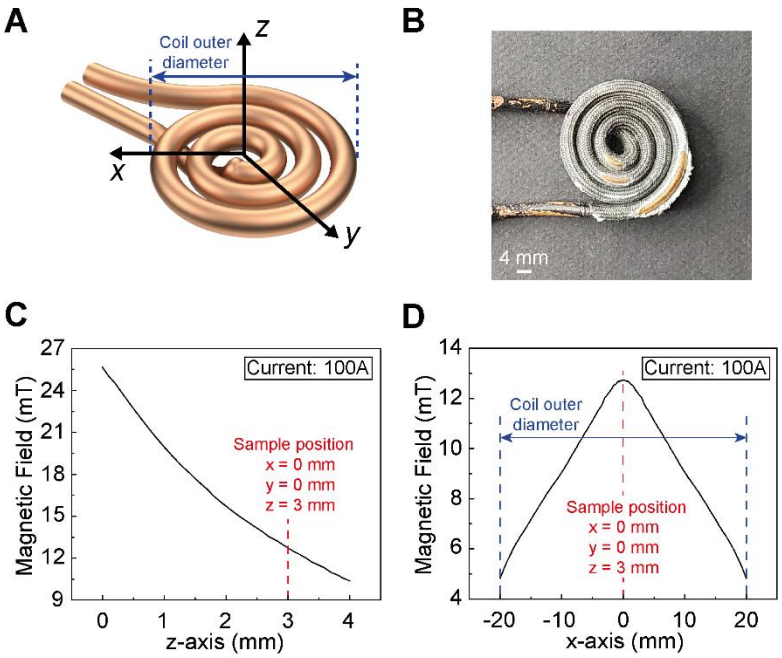

Figure S6. Magnetic field distribution of the spiral coil used in Figure 2D & Figure 3. (A) Schematic of the coil. The outer diameter of the coil is highlighted in dark blue. (B) Picture of the coil. Magnetic field distribution at a current of 100 A along (C) the z-axis, which is measured from the top surface of the coil, and (D) the x-axis, which is measured along the coil outer diameter. The sample position is highlighted in red on both curves.

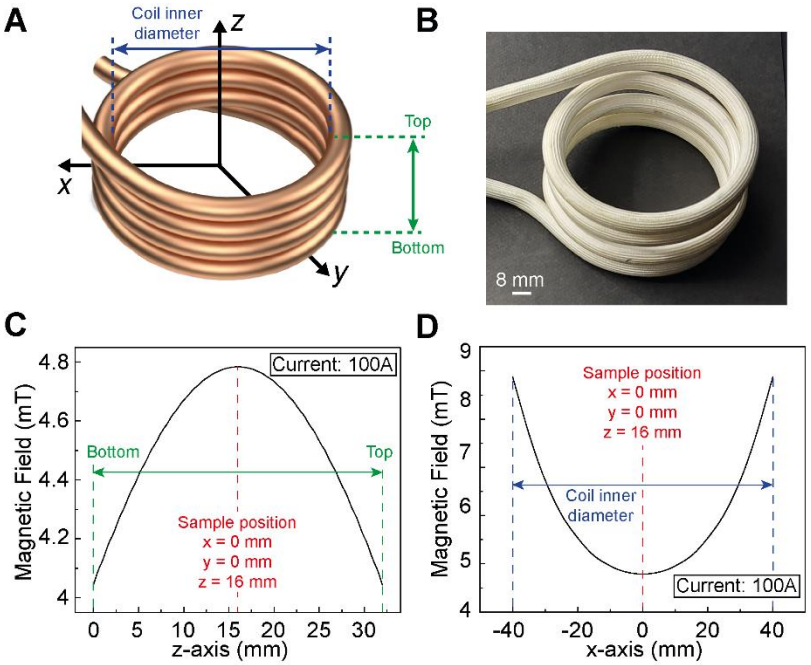

Figure S7. Magnetic field distribution of the helical coil used in Figure 2E. (A) Schematic of the coil. The inner diameter of the coil is highlighted in dark blue. The top and bottom of the coil are highlighted in green. (B) Picture of the coil. Magnetic field distribution at a current of 100 A along (C) the z-axis, which is measured from the bottom to the top of the coil, and (D) the x-axis, which is measured along the coil inner diameter. The sample position is highlighted in red on both curves.

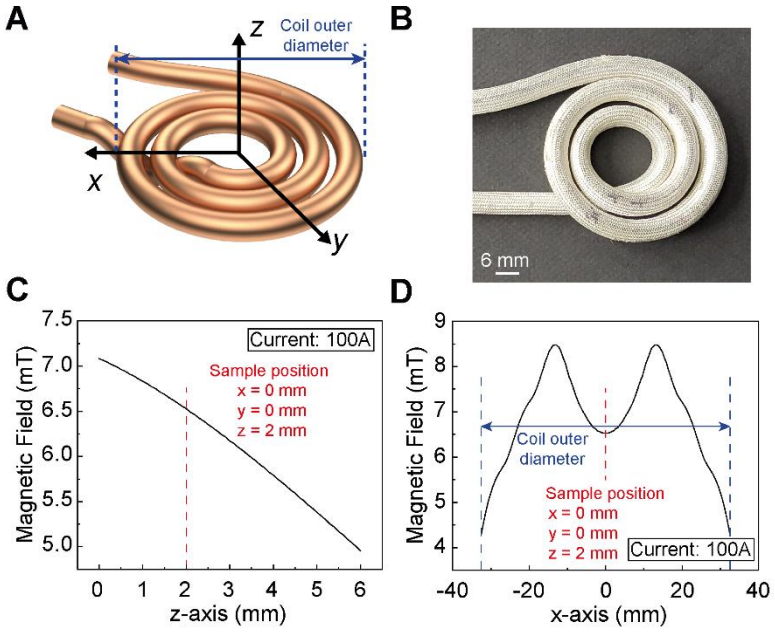

Figure S8. Magnetic field distribution of the spiral coil used in Figure 4. (A) Schematic of the coil. The outer diameter of the coil is highlighted in dark blue. (B) Picture of the coil. Magnetic field distribution at a current of 100 A along (C) the z-axis, which is measured from the top surface of the coil, and (D) the x-axis, which is measured along the coil outer diameter. The sample position is highlighted in red on both curves.

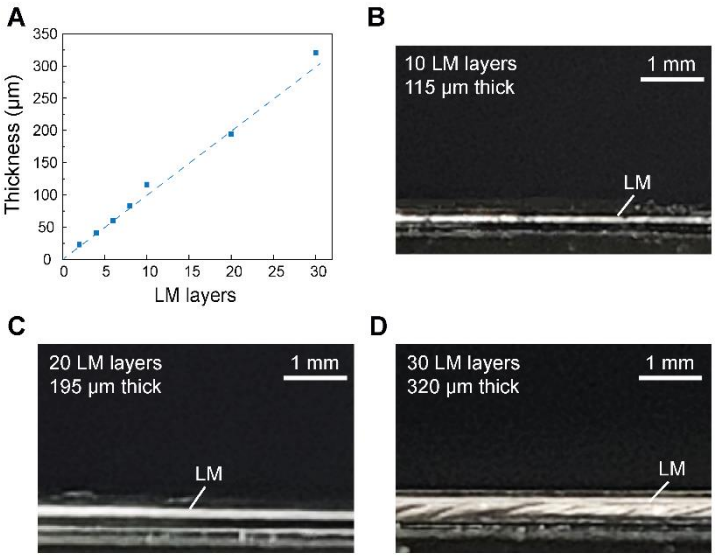

Figure S9. LM layer thickness characterization. (A) The thickness is linearly increasing with the number of LM layers sprayed, with each LM layer being ~10 µm thick. Pictures and measured thicknesses of the samples with (B) 10, (C) 20, and (D) 30 LM layers sandwiched between two glass slides. Scale bars: 1 mm.

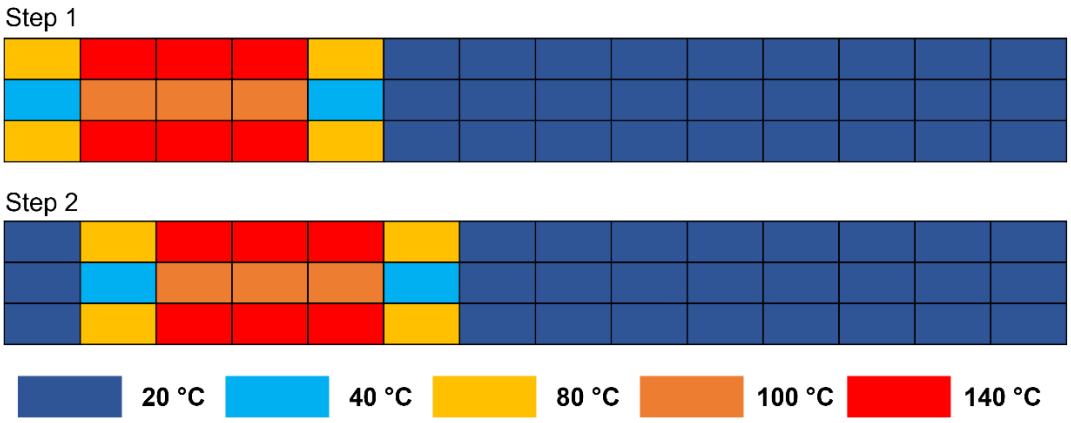

Figure S10. Temperature distribution schematic of the LCE-LM bilayer in thermo-structural FEA.

Supplementary Tables S1-S3

Table S1. Shapes and parameters of the different coils used for demonstrations.

Demonstration	Coil shape	D_o (mm)	D_i (mm)	n	f (kHz)	R (mΩ)
Actuation in Fig. 1E & F Sea turtle actuations in Fig. 5	Spiral	58	2	6	37	3.3
Heating in Fig. 2A, 2B & 2C	Helical	53	41	3	51	1.9
Selective heating in Fig. 2D Localized heating in Fig. 3	Spiral	40	2	4	46	2.4
Sequential heating in Fig. 2E	Helical	96	80	4	37	1.9
Sequential heating in Fig. 4	Spiral	65	25	3	60	1.5

D_o – Outer diameter of the coil
D_i – Inner diameter of the coil
n – Number of loops of the coil
f – Measured frequency of the generated alternating magnetic field
R – Measured resistance of the coils

Table S2. LM & coil properties used in the electromagnetic FEA

Materials	Relative permeability	Conductivity (S m^{-1})
LM (Galinstan)	0.6366	3.46×10^{6}
Coil (Copper)	0.999991	5.8×10^{7}

Table S3. LCE thermal expansion coefficients used in thermo-structural FEA

Alpha 11	Alpha 22	Alpha 33	Temperature (°C)
0	0	0	20
-0.001025	0.0005125	0.0005125	60
-0.0032	0.0016	0.0016	100
-0.002946	0.001473	0.001473	140

Supplementary Movies S1-S5

Movie S1 – Programmed actuation via modified LM patterns (Figure 1)

Movie S2 – Induction heating of LM with varying layers (Figure 2)

Movie S3 – Targeted actuation of the LCE-LM composite bilayer (Figure 3)

Movie S4 – Sequential actuation of the pop-up structure (Figure 4)

Movie S5 – Robotic sea turtle with omnidirectional locomotion (Figure 5)

References

[1] T. A. Kent, M. J. Ford, E. J. Markvicka, C. Majidi, *Multifunct. Mater.* **2020**, *3*, *025003.*

[2] A. Kotikian, J. M. Morales, A. Lu, J. Mueller, Z. S. Davidson, J. W. Boley, J. A. Lewis, *Adv. Mater.* **2021**, *33*, 1.